LETTER

doi:10.1038/nature26157

A new class of synthetic retinoid antibiotics effective against bacterial persisters

Wooseong Kim[1], Wenpeng Zhu[2], Gabriel Lambert Hendricks[1], Daria Van Tyne[3,4], Andrew D. Steele[5,6], Colleen E. Keohane[5,6], Nico Fricke[2], Annie L. Conery[7,8], Steven Shen[1], Wen Pan[1], Kiho Lee[1], Rajmohan Rajamuthiah[1], Beth Burgwyn Fuchs[1], Petia M. Vlahovska[9], William M. Wuest[5,6], Michael S. Gilmore[3,4], Huajian Gao[2], Frederick M. Ausubel[7,8] & Eleftherios Mylonakis[1]

A challenge in the treatment of *Staphylococcus aureus* infections is the high prevalence of methicillin-resistant *S. aureus* (MRSA) strains and the formation of non-growing, dormant 'persister' subpopulations that exhibit high levels of tolerance to antibiotics[1–3] and have a role in chronic or recurrent infections[4,5]. As conventional antibiotics are not effective in the treatment of infections caused by such bacteria, novel antibacterial therapeutics are urgently required. Here we used a *Caenorhabditis elegans*–MRSA infection screen[6] to identify two synthetic retinoids, CD437 and CD1530, which kill both growing and persister MRSA cells by disrupting lipid bilayers. CD437 and CD1530 exhibit high killing rates, synergism with gentamicin, and a low probability of resistance selection. All-atom molecular dynamics simulations demonstrated that the ability of retinoids to penetrate and embed in lipid bilayers correlates with their bactericidal ability. An analogue of CD437 was found to retain anti-persister activity and show an improved cytotoxicity profile. Both CD437 and this analogue, alone or in combination with gentamicin, exhibit considerable efficacy in a mouse model of chronic MRSA infection. With further development and optimization, synthetic retinoids have the potential to become a new class of antimicrobials for the treatment of Gram-positive bacterial infections that are currently difficult to cure.

We used an established automated high-throughput *C. elegans*–MRSA killing assay in 384-well plates[6] to screen approximately 82,000 small synthetic molecules, and identified 185 compounds that significantly decreased the ability of MRSA to kill the nematodes (Fig. 1a, Supplementary Table 1, Supplementary Methods). Two of these 185 compounds, the synthetic retinoids CD437 and CD1530 (vitamin A analogues; Fig. 1b), were selected for further investigation because they have similar structures and have been studied previously for their therapeutic potential[7–10].

CD437 and CD1530 exhibit potent *in vitro* bactericidal activity against MRSA strain MW2; after two hours, levels of MW2 were below the limit of detection (minimum inhibitory concentration (MIC) 1 μg ml^{-1}; Fig. 1c, Extended Data Fig. 1a, Supplementary Table 2). *In vivo*, CD437 or CD1530 at concentrations above their *in vitro* MICs protected 100% of *C. elegans* against MW2-induced death (Fig. 1d). CD437 and CD1530 also exhibited potent activity against a panel of clinical *S. aureus* and *Enterococcus faecium* strains, but not against Gram-negative species (Supplementary Table 2). In addition, adarotene, a structural analogue of CD437 and CD1530 and a potential ovarian cancer drug[8] (Fig. 1b), also exhibited significant anti-staphylococcal activity (MIC 2 μg ml^{-1}) and prevented the MRSA-induced death of *C. elegans*. However, adapalene, another analogue and a US Food and Drug Administration (FDA)-approved acne therapeutic[11], was ineffective against MRSA (Fig. 1a–d, Extended Data Fig. 1a, Supplementary Table 2).

We were unable to obtain retinoid-resistant mutants by plating 10^{10} colony-forming units (CFU) of *S. aureus* MW2 on agar containing 2.5×, 5× or 10× MIC of CD437, CD1530 or adarotene. Similarly, serial passage of two independent *S. aureus* MW2 cultures (SP1 and SP2) for 100 days in sub-MIC levels of CD437 yielded only putative mutants with twofold greater resistance to CD437, CD1530 or adarotene, whereas serial passage in ciprofloxacin for 100 days (Fig. 1e) or daptomycin for 15 days (Extended Data Fig. 1b) generated strains that were 256-fold and tenfold more resistant, respectively. The MW2 cultures that exhibited modest retinoid resistance contained mutations in the genes *graS*, *yjbH* and *manA* (Fig. 1f, Supplementary Tables 3–5, Supplementary Discussion), which encode products related to membrane physiology[12–16]. Consistent with this finding, CD437, CD1530 and adarotene—but not adapalene—induced membrane permeabilization in MW2 (monitored by SYTOX Green uptake; Fig. 2a), and CD437 and CD1530 caused the formation of mesosome-like structures (observed by transmission electron microscopy; Fig. 2b), similar to those observed in *S. aureus* cells after treatment with antimicrobial peptides[17]. Moreover, CD437, CD1530 and adarotene disrupted the integrity of biomembrane-mimicking giant unilamellar vesicles (Fig. 2c, Supplementary Videos 1–5). These vesicles consist of a DOPC:DOPG lipid bilayer at a ratio of 7:3 (DOPC/G, 1,2-dioleoyl-*sn*-glycero-3-phosphocholine/glycerol), which mimics anionic bacterial membranes, and have been used to elucidate the mechanisms of action of daptomycin in *S. aureus*[18,19]. Notably, however, CD437 and CD1530 did not lyse bacterial cells directly (Extended Data Fig. 1c).

To elucidate the molecular interactions between retinoids and the membrane lipid bilayers of *S. aureus*, we conducted all-atom molecular dynamics simulations using a lipid bilayer composed of 108 phosphatidylglycerol lipids, 72 lysyl-phosphatidylglycerol (Lys-PG) lipids and 10 diphosphatidylglycerol (DPG, also known as cardiolipin) lipids, which mimics the phospholipid composition of *S. aureus* membranes[20]. These simulations showed that the carboxylic acid and the phenolic groups of CD437, CD1530 and adarotene anchor these retinoids to the surface of the membrane bilayer by binding persistently to hydrophilic lipid heads. As a result, the retinoids penetrate the bilayers and become embedded orthogonally to the lipid molecules in the outer membrane leaflet, inducing substantial perturbations of the membrane (Fig. 2d, e, Supplementary Videos 6–9). Similar results were obtained for molecular dynamics simulations of DOPC:DOPG (7:3) lipid bilayers used in the giant unilamellar vesicle experiments in Fig. 2c (Extended Data Fig. 2a, b, Supplementary Videos 10–13). In contrast to CD437, CD1530 and adarotene, adapalene does not penetrate the membrane owing to a high energy barrier (11.22 k_BT) and an unfavourable

[1]Division of Infectious Diseases, Rhode Island Hospital, Warren Alpert Medical School of Brown University, Providence, Rhode Island 02903, USA. [2]School of Engineering, Brown University, Providence, Rhode Island 02903, USA. [3]Department of Ophthalmology, Harvard Medical School, Massachusetts Eye and Ear Infirmary, Boston, Massachusetts 02114, USA. [4]Department of Microbiology and Immunobiology, Harvard Medical School, Massachusetts 02115, USA. [5]Department of Chemistry, Emory University, Atlanta, Georgia 30322, USA. [6]Emory Antibiotic Resistance Center, Emory University, Atlanta, Georgia 30322, USA. [7]Department of Molecular Biology, Massachusetts General Hospital, Boston, Massachusetts 02114, USA. [8]Department of Genetics, Harvard Medical School, Boston, Massachusetts 02115, USA. [9]Department of Engineering Sciences and Applied Mathematics, Northwestern University, Evanston, Illinois 60208, USA.

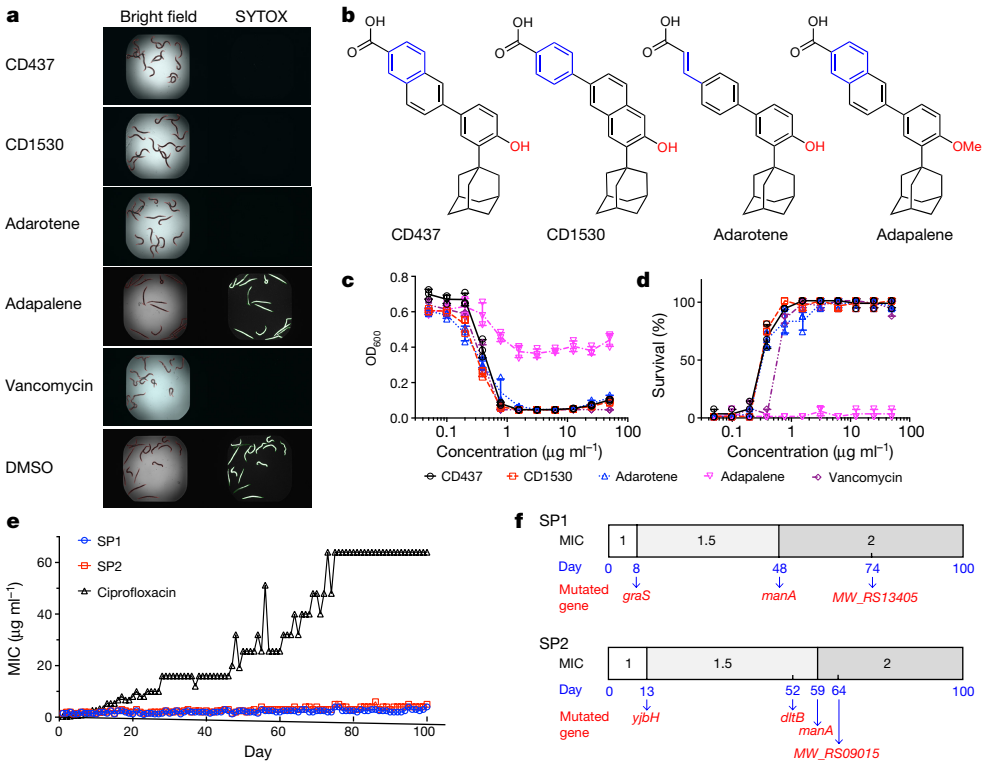

Figure 1 | Synthetic retinoids protect *C. elegans* from MRSA infection and inhibit MRSA growth without detectable mutant development. **a**, Images of MRSA-MW2-infected *C. elegans* in the presence of 10 μg ml^{-1} retinoids, 10 μg ml^{-1} vancomycin, or 1% DMSO as a control (see Supplementary Methods). Only dead worms stain with SYTOX Orange. Experiments were independently repeated three times with similar results. **b**, Chemical structures of synthetic retinoids. **c**, Growth of MW2 exposed to the five indicated compounds at various concentrations after 18 hours in tryptic soy broth. OD_{600}, optical density at 600 nm. **d**, Survival of *C. elegans* infected with MW2 in the presence of retinoids, normalized to *C. elegans* treated with DMSO. **c**, **d**, Individual data points ($n = 3$ biologically independent experiments) and mean ± s.d. are shown. **e**, Appearance of spontaneous CD437- and ciprofloxacin-resistant MW2 mutants over 100 days of serial passage in duplicate (SP1 and SP2) (see Supplementary Methods). **f**, Appearance of mutations on specific days in the indicated genes in SP1 and SP2 in **e** (see Supplementary Methods). The modest increase in the MIC of CD437 against MRSA during serial passage was confirmed by remeasuring MICs using three colonies from aliquots of each passage that had been stored at −80 °C. Mutated genes are indicated on the day at which the mutations were first detected.

transfer energy (3.16 k_BT) (Fig. 2e, Supplementary Table 6), as the hydrophobic methoxy group does not bind to lipid heads (Fig. 2d, Supplementary Video 9). CD437-like retinoids can be metabolized in the liver by glucuronidation at carboxylic or hydroxyl groups[21]. Molecular dynamics simulations showed that two CD437 glucuronide metabolites also penetrate into lipid bilayers, exhibiting a similar penetration mechanism to that of CD437 (Extended Data Fig. 2a, c, Supplementary Videos 14, 15, Supplementary Discussion). In summary, these molecular dynamics simulations showed that two polar branch groups—a phenol and a carboxylate—have essential roles in membrane attachment and penetration, and that the membrane activity of retinoids (Fig. 2) directly correlates with their antibiotic activity (Fig. 1c, Extended Data Fig. 1a).

CD437 or CD1530—but not adarotene—also induced rapid permeabilization of MRSA-persister membranes (Extended Data Fig. 3a), and killed MRSA-persister cells (Fig. 3a, Extended Data Fig. 3b). They also completely eradicated persisters formed by 13 clinical isolates, including the multi-drug resistant strain VRS1 within 1 to 4 hours at 8–10× MIC (Fig. 3b, Extended Data Fig. 3c, d). Moreover, CD437 or CD1530 killed around 90% and 100% of persisters formed in MRSA biofilms at 16× MIC and 32× MIC, respectively (Extended Data Fig. 4). Compared with adarotene, CD437 and CD1530 can penetrate the membrane more efficiently owing to lower energy barriers and more favourable transfer energies (Fig. 2e); this is consistent with the observation that adarotene is inactive against persister cells. The results suggest that the planar aryl moiety of CD437 and CD1530 (highlighted in blue, Fig. 1b) rigidifies the carboxylic acid, which facilitates penetration into lipid bilayers, whereas the flexible cinnamoyl moiety of adarotene fails to orient the carboxylate appropriately, thereby decreasing membrane penetration (Fig. 2e).

CD437 or CD1530 exhibited significant synergism with gentamicin against both MRSA growing and persister cells (Fig. 3c, Supplementary Table 7, Extended Data Fig. 4). This is most probably a consequence of the increased passive diffusion of gentamicin through the bacterial cell membranes that have been physically damaged by the retinoids, which is mechanistically distinct from the observed synergism between gentamicin and ionophores[22] (Extended Data Fig. 5, Supplementary Discussion).

Although membrane-targeting agents often cause toxicity in mammals[23], CD437, CD1530 and adarotene are relatively non-toxic, exhibiting median haemolytic concentrations (HC_{50}) of greater than 32 μg ml^{-1} (Extended Data Fig. 6a). CD437, CD1530 and adarotene were more toxic to human hepatoma HepG2 cells (median lethal concentration (LC_{50}) 3–5 μg ml^{-1}) than to normal human primary hepatocytes ($LC_{50} \geq 20$ μg ml^{-1}), or to primary renal proximal tubule epithelial cells or adult normal human epidermal keratinocytes at 8 μg ml^{-1} (Extended Data Fig. 6b), a concentration at which CD437 and CD1530 completely eradicated MRSA persisters (Fig. 3a). These data are consistent with previous results showing that CD437 exhibits selective toxicity towards cancer cells[10]. None of the three retinoids inhibited the human ether-a-go-go related (hERG) potassium channels that are critical for cardiac action potential repolarization at 25 μM (Extended Data Fig. 6c) and did not show significant genotoxic potential (Supplementary Table 8).

To evaluate the effects of the CD437-like retinoid branch groups on antimicrobial activity and the possibility of further structural

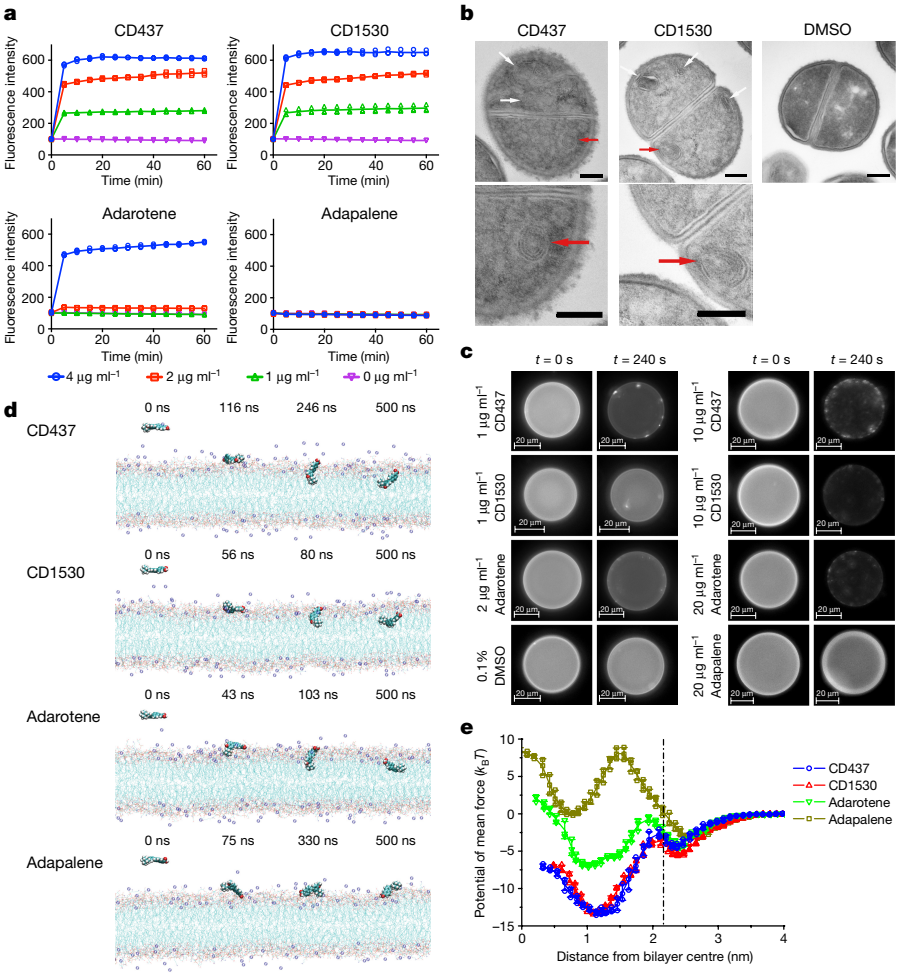

Figure 2 | CD437, CD1530 and adarotene disrupt membrane lipid bilayers. a, Uptake of SYTOX Green ($\lambda_{ex} = 485$ nm, $\lambda_{em} = 525$ nm) by exponential-phase *S. aureus* MW2 cells treated with retinoids. Individual data points ($n = 3$ biologically independent samples) and means are shown. Error bars not shown for clarity. **b**, Transmission electron micrographs showing mesosome-like structures (white and red arrows; enlarged in bottom images) in 10× MIC retinoid-treated cells and DMSO control. Scale bars, 200 nm. **c**, Changes in giant unilamellar vesicles (DOPC:DOPG. 7:3) labelled with 18:1 Liss Rhod PE (0.05%) treated with retinoids or with 0.1% DMSO, monitored using fluorescence microscopy (40× objective, $\lambda_{ex} = 460$ nm, $\lambda_{em} = 483$ nm). Liss Rhod PE, 1,2-dioleoyl-*sn*-glycero-3-phosphoethanolamine-*N*-(lissamine rhodamine B sulfonyl) (ammonium salt). In **b**, **c**, experiments were independently repeated twice with similar results. **d**, Representative configurations of molecular dynamics simulations of retinoids at, from left to right, onset, membrane attachment, membrane penetration and equilibrium interacting with lipid bilayers (membrane composition: 108 phosphatidylglycerol lipids, 72 Lys-PG lipids, and 10 DPG lipids; see Supplementary Methods for atomic rendering). Simulations were repeated five times with similar results. **e**, Free-energy profiles of retinoids penetrating the membrane as a function of the distance between the centre-of-mass (COM) of the retinoid and the lipid bilayer. The dot-dashed line marks the membrane surface, averaged from the COM location of phosphate groups in outer leaflet. Individual data points ($n = 3$ independent simulations) and mean ± s.d. are shown.

optimization with respect to antimicrobial and toxicity profiles, we synthesized 16 analogues of CD437 (Extended Data Fig. 7a). Subsequent analysis of their structure–activity relationships supported the putative mode of action by which the synthetic retinoids disrupt Gram-positive bacterial membranes, and demonstrated that the antimicrobial activity and cytotoxicity of synthetic retinoids can be modulated by the polarity of the branch groups (Extended Data Figs 7–9, Supplementary Videos 16, 17, Supplementary Discussion). In particular, analogue 2, which has a less polar primary alcohol instead of the carboxylic acid group, retained bacterial activity against MRSA persisters (Fig. 4a, b), but showed significantly less haemolytic activity ($HC_{50} > 32\,\mu g\,ml^{-1}$, Extended Data Fig. 8a) and less cytotoxicity in a panel of human cell lines ($LC_{50} \geq 31\,\mu g\,ml^{-1}$) than did CD437 (Fig. 4c, Extended Data Fig. 6b). Analogue 2 also showed significantly reduced activity towards human hepatoma HepG2 cells, with LC_{50} values of $>32\,\mu g\,ml^{-1}$ (Fig. 4c). In addition, molecular dynamics simulations revealed that analogue 2 penetrates membrane lipid bilayers with similar energy profiles to those of CD437 (Extended Data Fig. 8d, e, Supplementary Video 16), further establishing that the extent of membrane penetration inferred from molecular dynamics simulations correlates with antimicrobial activity. In summary, the structure–activity relationships verified that persistent attachment to lipid heads by the two polar branch groups is critical for antimicrobial activity, and that antimicrobial activity and lack of cytotoxicity can be optimized by simple modifications to the polar branch groups. Notably, analogue 2 also exhibited favourable pharmacokinetic profiles after intraperitoneal administration of a single dose of 20 mg kg^{-1}, with a maximum plasma concentration of around 10 μg ml^{-1} and an elimination half-life of 4.5 hours (Extended Data Fig. 8f). By contrast, adarotene is excreted rapidly[21,24]. Analogue 2 showed no detectable hepatic or renal toxicity in mice at intraperitoneal doses of up to 80 mg kg^{-1} (the highest tested dose) every 12 hours for 3 days (Extended Data Fig. 8g).

Finally, we evaluated the efficacy of both analogue 2 and the combination of analogue 2 and gentamicin in a mouse deep-seated thigh MRSA infection model, which mimics human deep-seated chronic infections[2]. Consistent with previous findings[2], a combination of vancomycin and

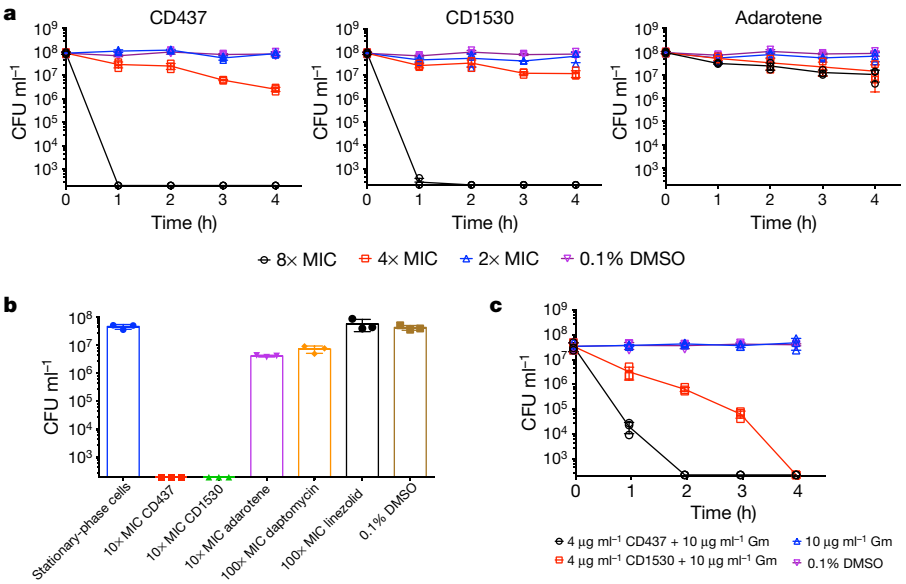

Figure 3 | CD437 or CD1530 alone or in combination with gentamicin are effective against persisters. a, **b**, Viability of stationary-phase *S. aureus* MW2 (**a**) or *S. aureus* VRS1 (**b**) when treated with the indicated concentrations of each retinoid for 4 hours. **c**, Viability upon treatment of *S. aureus* MW2 persisters with the indicated concentrations of retinoids in combination with gentamicin (Gm). In **a**–**c**, the data points on the *x* axis are below the level of detection (2×10^2 CFU ml^{-1}). Individual data points ($n = 3$ biologically independent samples) and mean ± s.d. are shown.

gentamicin did not significantly reduce MRSA abundance (Fig. 4d) even though MW2 is sensitive to both antibiotics, which suggests that the bacterial cells in this infection model are persisters. As shown in Fig. 4d, 80 mg kg^{-1} of analogue 2 alone led to an approximately fourfold decrease ($P < 0.001$) in MRSA abundance, and 40 or 80 mg kg^{-1} of analogue 2 in combination with 30 mg kg^{-1} gentamicin resulted in approximately 14-fold ($P < 0.001$) and approximately 23-fold decreases ($P < 0.001$) in bacterial burden, respectively. Similarly, CD437 alone or

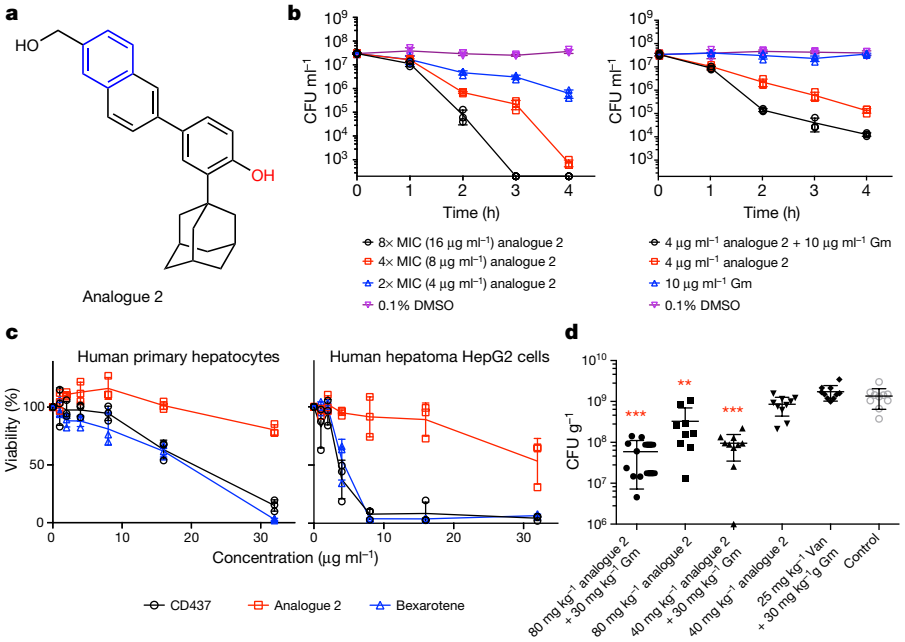

Figure 4 | Analogue 2 retains antimicrobial activity against MRSA persisters and has improved cytotoxicity compared with CD437. **a**, Chemical structure of analogue 2. **b**, Viability of *S. aureus* MW2 persisters treated with analogue 2 alone or in combination with gentamicin (Gm). Data points on the *x* axis were below the level of detection (2×10^2 CFU ml^{-1}). **c**, Viability of normal human primary hepatocytes and human hepatoma (HepG2) cells treated with retinoids in serum-free medium for 24 hours, based on the absorbance readings at 450 nm taken 4 hours after adding the tetrazolium dye WST-1. The FDA-approved antineoplastic retinoid bexarotene was used as a control. **b**, **c**, Individual data points ($n = 3$ biologically independent samples) and mean ± s.d. are shown. **d**, Efficacy of analogue 2 alone or in combination with gentamicin in a deep-seated mouse thigh infection model. Each group of MW2-infected neutropenic mice ($n = 10$ biologically independent animals) was treated with the indicated doses of analogue 2 intraperitoneally (i.p.) alone or in combination with 30 mg kg^{-1} subcutaneous (s.c.) gentamicin (Gm), a combination of 25 mg kg^{-1} vancomycin (Van, i.p.) and 30 mg kg^{-1} gentamicin (s.c.) or control (5% Kolliphor + 5% ethanol, i.p.) every 12 hours for 3 days beginning 24 hours after infection. At 12 hours after the last treatment, mice were euthanized and their thighs were excised and homogenized. CFUs from each mouse thigh are plotted as individual points. The mean ± s.d. is shown. Statistical differences between control and antibiotic treatment groups were analysed by one-way ANOVA and post hoc Tukey test (**$P = 0.0002$, ***$P < 0.0001$).

in combination with gentamicin also exhibited efficacy in the MRSA mouse deep-seated thigh infection model (Extended Data Fig. 10). These results suggest that a combination of analogue 2 and gentamicin or CD437 and gentamicin might be an effective strategy to enhance the efficacy and reduce the toxicity of aminoglycosides[25] in the treatment of chronic Gram-positive infections.

Despite the potential advantages of membrane-active antimicrobials such as the retinoids described here—including fast killing, low probability of developing resistance, and anti-persister activity—the major obstacle for developing retinoids as therapeutics is their potential cytotoxicity, which is a matter of considerable debate[23,26]. Nevertheless, we have identified a specific chemotype of membrane-active synthetic retinoids that are relatively selective for bacterial membranes and exhibit a high level of activity towards MRSA persister cells; these findings are notable because the development of appropriate antibiotics for persisters is an important unmet need. Although a limited analysis of structure–activity relationships showed that modification of the retinoid branch groups can result in improved cytotoxicity profiles while retaining anti-persister activity, it is important to acknowledge that the long term-potential of further chemical optimization of retinoids to develop non-toxic antimicrobials is currently unknown. However, considering the fact that the bioactivity of retinoids can be improved by modifying both the backbone and branch groups, and that approximately 4,000 retinoid analogues have been synthesized so far[26], our results warrant further development of synthetic retinoids as potential therapeutics for hard-to-treat infectious diseases caused by antibiotic-resistant or persistent Gram-positive pathogens.

Data Availability All data are available within the paper and its Supplementary Information.

Online Content Methods, along with any additional Extended Data display items and Source Data, are available in the online version of the paper; references unique to these sections appear only in the online paper.

Received 31 August 2016; accepted 26 February 2018.
Published online 28 March 2018.

1. Allison, K. R., Brynildsen, M. P. & Collins, J. J. Metabolite-enabled eradication of bacterial persisters by aminoglycosides. *Nature* **473,** 216–220 (2011).
2. Conlon, B. P. *et al.* Activated ClpP kills persisters and eradicates a chronic biofilm infection. *Nature* **503,** 365–370 (2013).
3. Davies, J. & Davies, D. Origins and evolution of antibiotic resistance. *Microbiol. Mol. Biol. Rev.* **74,** 417–433 (2010).
4. Lew, D. P. & Waldvogel, F. A. Osteomyelitis. *Lancet* **364,** 369–379 (2004).
5. Baddour, L. M. *et al.* Infective endocarditis in adults: diagnosis, antimicrobial therapy, and management of complications: a scientific statement for healthcare professionals from the American Heart Association. *Circulation* **132,** 1435–1486 (2015).
6. Rajamuthiah, R. *et al.* Whole animal automated platform for drug discovery against multi-drug resistant *Staphylococcus aureus*. *PLoS ONE* **9,** e89189 (2014).
7. Altucci, L., Leibowitz, M. D., Ogilvie, K. M., de Lera, A. R. & Gronemeyer, H. RAR and RXR modulation in cancer and metabolic disease. *Nat. Rev. Drug Discov.* **6,** 793–810 (2007).
8. Valli, C. *et al.* Atypical retinoids ST1926 and CD437 are S-phase-specific agents causing DNA double-strand breaks: significance for the cytotoxic and antiproliferative activity. *Mol. Cancer Ther.* **7,** 2941–2954 (2008).
9. Tang, X.-H. *et al.* Combination of bexarotene and the retinoid CD1530 reduces murine oral-cavity carcinogenesis induced by the carcinogen 4-nitroquinoline 1-oxide. *Proc. Natl Acad. Sci. USA* **111,** 8907–8912 (2014).
10. Han, T. *et al.* The antitumor toxin CD437 is a direct inhibitor of DNA polymerase α. *Nat. Chem. Biol.* **12,** 511–515 (2016).
11. Irby, C. E., Yentzer, B. A. & Feldman, S. R. A review of adapalene in the treatment of acne vulgaris. *J. Adolesc. Health* **43,** 421–424 (2008).
12. Meehl, M., Herbert, S., Götz, F. & Cheung, A. Interaction of the GraRS two-component system with the VraFG ABC transporter to support vancomycin-intermediate resistance in *Staphylococcus aureus*. *Antimicrob. Agents Chemother.* **51,** 2679–2689 (2007).
13. Yang, S.-J. *et al.* The *Staphylococcus aureus* two-component regulatory system, GraRS, senses and confers resistance to selected cationic antimicrobial peptides. *Infect. Immun.* **80,** 74–81 (2012).
14. Elbaz, M. & Ben-Yehuda, S. The metabolic enzyme ManA reveals a link between cell wall integrity and chromosome morphology. *PLoS Genet.* **6,** e1001119 (2010).
15. Falord, M., Mäder, U., Hiron, A., Débarbouillé, M. & Msadek, T. Investigation of the *Staphylococcus aureus* GraSR regulon reveals novel links to virulence, stress response and cell wall signal transduction pathways. *PLoS ONE* **6,** e21323 (2011).
16. Göhring, N. *et al.* New role of the disulfide stress effector YjbH in β-lactam susceptibility of *Staphylococcus aureus*. *Antimicrob. Agents Chemother.* **55,** 5452–5458 (2011).
17. Friedrich, C. L., Moyles, D., Beveridge, T. J. & Hancock, R. E. Antibacterial action of structurally diverse cationic peptides on gram-positive bacteria. *Antimicrob. Agents Chemother.* **44,** 2086–2092 (2000).
18. Chen, Y.-F., Sun, T.-L., Sun, Y. & Huang, H. W. Interaction of daptomycin with lipid bilayers: a lipid extracting effect. *Biochemistry* **53,** 5384–5392 (2014).
19. Ganewatta, M. S. *et al.* Bio-inspired resin acid-derived materials as anti-bacterial resistance agents with unexpected activities. *Chem. Sci.* **5,** 2011–2016 (2014).
20. Piggot, T. J., Holdbrook, D. A. & Khalid, S. Electroporation of the *E. coli* and *S. aureus* membranes: molecular dynamics simulations of complex bacterial membranes. *J. Phys. Chem. B* **115,** 13381–13388 (2011).
21. Sala, F. *et al.* Development and validation of a liquid chromatography–tandem mass spectrometry method for the determination of ST1926, a novel oral antitumor agent, adamantyl retinoid derivative, in plasma of patients in a Phase I study. *J. Chromatogr. B* **877,** 3118–3126 (2009).
22. Farha, M. A., Verschoor, C. P., Bowdish, D. & Brown, E. D. Collapsing the proton motive force to identify synergistic combinations against *Staphylococcus aureus*. *Chem. Biol.* **20,** 1168–1178 (2013).
23. Hurdle, J. G., O'Neill, A. J., Chopra, I. & Lee, R. E. Targeting bacterial membrane function: an underexploited mechanism for treating persistent infections. *Nat. Rev. Microbiol.* **9,** 62–75 (2011).
24. Basma, H. *et al.* The synthetic retinoid ST1926 as a novel therapeutic agent in rhabdomyosarcoma. *Int. J. Cancer* **138,** 1528–1537 (2016).
25. Cosgrove, S. E. *et al.* Initial low-dose gentamicin for *Staphylococcus aureus* bacteremia and endocarditis is nephrotoxic. *Clin. Infect. Dis.* **48,** 713–721 (2009).
26. Álvarez, R., Vaz, B., Gronemeyer, H. & de Lera, A. R. Functions, therapeutic applications, and synthesis of retinoids and carotenoids. *Chem. Rev.* **114,** 1–125 (2014).

Supplementary Information is available in the online version of the paper.

Acknowledgements This study was supported by National Institutes of Health grant P01 AI083214 to M.S.G., F.M.A. and E.M., by National Science Foundation grant CMMI-1562904 to H.G., and by National Institute of General Medical Sciences grant 1R35GM119426 and National Science Foundation grant NSF1755698 to W.M.W. D.V.T. is supported by National Eye Institute grant EY028222. We thank the Institute of Chemistry and Cell Biology-Longwood at Harvard Medical School for providing the chemical libraries used in this study. We thank L. Rice for providing the *E. faecium* strains, K. Bayles and J. Endres for providing plasmid pBK123, J. Saavedra for assistance with next-generation sequencing library preparation, and S. Khalid for providing the atomic structures and force fields of the phosphatidylglycerol, Lys-PG and DPG lipids. The simulations reported were performed on resources provided by the Extreme Science and Engineering Discovery Environment through grant MSS090046 and the Center for Computation and Visualization at Brown University.

Author Contributions W.K., A.L.C., R.R., B.B.F., F.M.A. and E.M. designed the chemical screen. W.K., B.B.F. and R.R. performed the chemical screen. W.K. designed, performed and analysed MIC assays, dose–response *C. elegans* infection assays, membrane permeability assays, time-kill assays and transmission electron microscopy experiments. W.K. and D.V.T. designed, performed and analysed the selection of resistant mutants and whole genome sequencing. W.K., N.F. and P.M.V. designed, performed and analysed giant unilamellar vesicle experiments. W.K., W.Z. and H.G. designed, performed and analysed molecular dynamics simulations. A.D.S., C.E.K. and W.M.W. synthesized analogues. W.K. and B.B.F. designed, performed and analysed toxicity tests. W.K., G.L.H., S.S., W.P. and K.L. designed, performed and analysed animal studies. A.L.C., B.B.F., P.M.V., W.M.W., M.S.G., H.G., F.M.A. and E.M. contributed reagents, materials and/or analysis tools. E.M. supervised the project. W.K., W.Z., G.L.H., W.M.W., H.G., F.M.A. and E.M. wrote the manuscript.

Author Information Reprints and permissions information is available at www.nature.com/reprints. The authors declare competing interests: details are available in the online version of the paper. Readers are welcome to comment on the online version of the paper. Publisher's note: Springer Nature remains neutral with regard to jurisdictional claims in published maps and institutional affiliations. Correspondence and requests for materials should be addressed to E.M. (emylonakis@lifespan.org).

Reviewer Information *Nature* thanks F. DeLeo and the other anonymous reviewer(s) for their contribution to the peer review of this work.

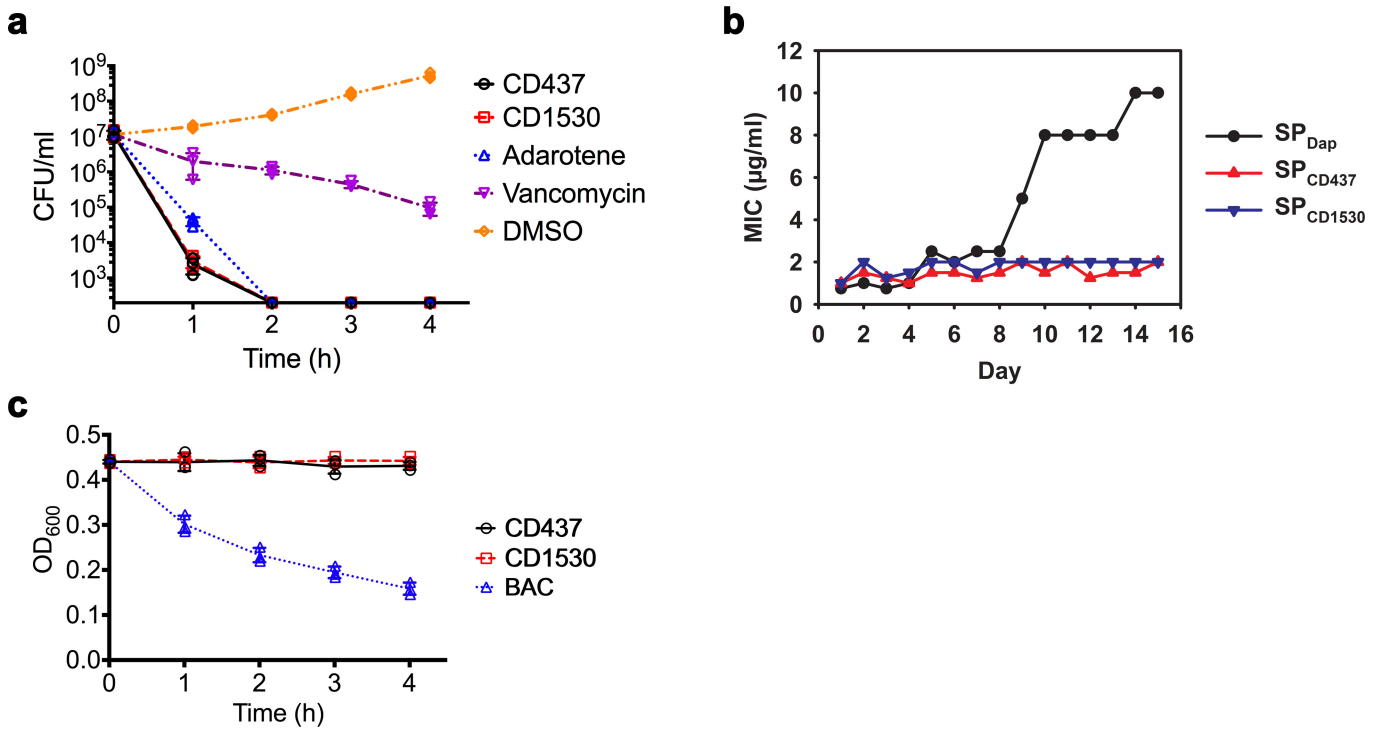

Extended Data Figure 1 | CD437 and CD1530 show fast-killing kinetics and low probability of resistance development, and do not cause detectable cell lysis. a, Exponential-phase MRSA cells (strain MW2) were treated with 10× MIC CD437, CD1530, adarotene, vancomycin or 0.1% DMSO (negative control). CFU counts of cells were measured by serial dilution and plating on agar plates. The data points on the *x* axis are below the level of detection (2×10^2 CFU ml^{-1}). Individual data points ($n = 3$ biologically independent samples) and mean ± s.d. are shown. **b**, Development of *S. aureus* MW2 mutants resistant to CD437 (SP_{CD437}), CD1530 (SP_{CD1530}) or daptomycin (SP_{Dap}) was attempted by daily serial passage for 15 days. **c**, Exponential-phase *S. aureus* MW2 bacteria were treated with 10× MIC CD437, CD1530 or benzalkonium chloride (BAC) for 4 h. The anti-infective detergent BAC was used as a positive control for cell lysis. OD_{600} was measured in a spectrophotometer every hour. Individual data points ($n = 3$ biologically independent samples) and mean ± s.d. are shown.

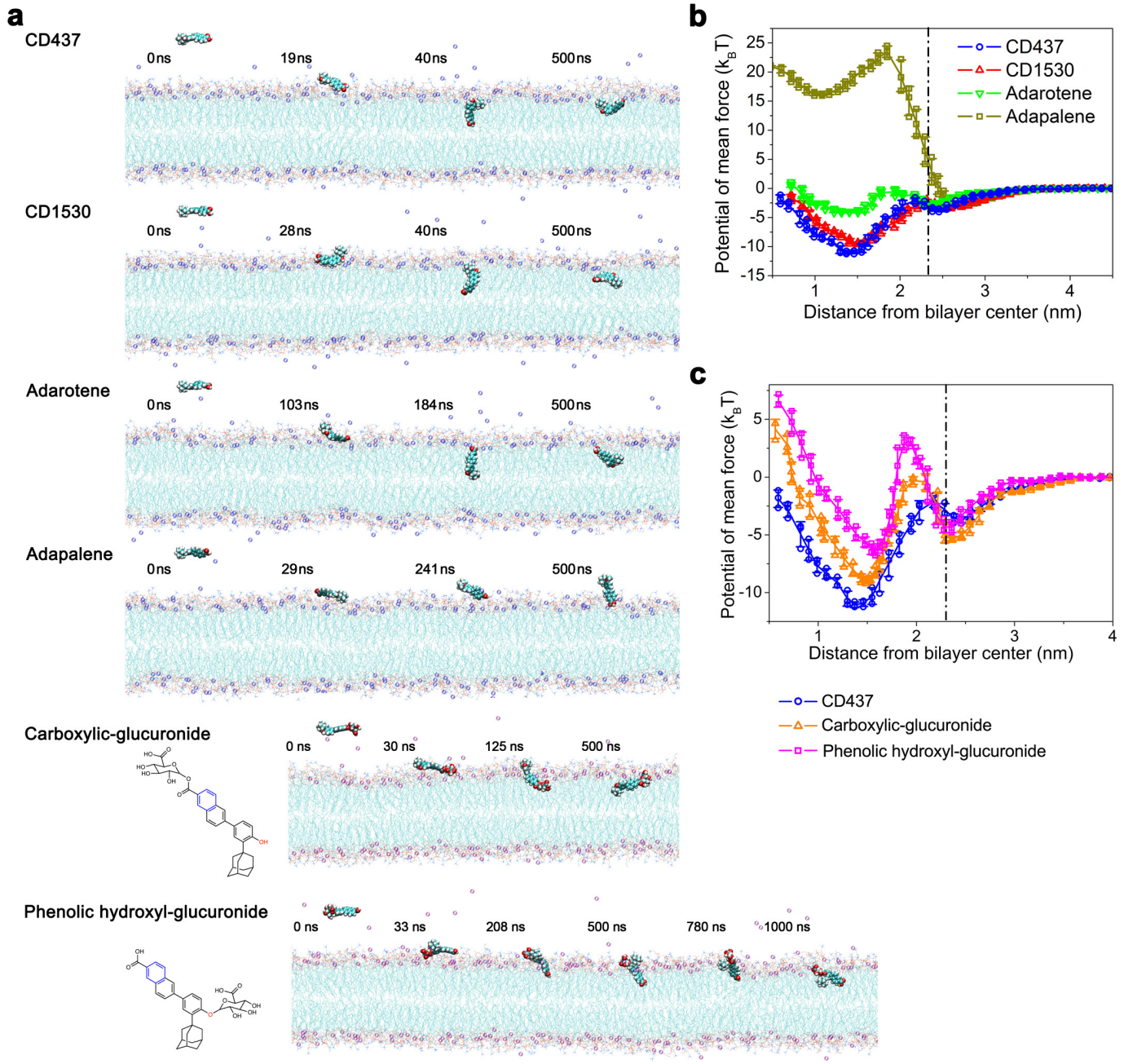

Extended Data Figure 2 | All-atom molecular dynamics simulations showing the interactions between selected retinoids or retinoid metabolites and a DOPC:DOPG (7:3) lipid bilayer. a, Representative configurations of synthetic retinoids or retinoid metabolites at, left to right, the onset of simulation, membrane attachment, membrane penetration and equilibrium state (see Supplementary Methods for atomic rendering). Simulations were repeated five times with similar results. **b**, **c**, Free energy profiles of the four retinoids (**b**) or CD437-metabolites (**c**) penetrating the membrane as a function of the distance between the COM of the retinoids or the retinoid metabolites and the lipid bilayer. The dot-dashed line marks the membrane surface, averaged from the COM location of phosphate groups in the outer leaflet. Individual data points ($n = 3$ independent simulations) and mean ± s.d. are shown. The membrane penetration of CD437, CD1530, adarotene, adapalene, the carboxylic-glucuronide metabolite and the phenolic hydroxyl-glucuronide metabolite are associated with transfer energies of $-8.92\ k_BT$, $-7.14\ k_BT$, $-1.45\ k_BT$, $18.76\ k_BT$, $-3.73\ k_BT$, $-2.02\ k_BT$ and energy barriers of $1.42\ k_BT$, $1.12\ k_BT$, $2.03\ k_BT$, $26.13\ k_BT$, $5.01\ k_BT$, $7.40\ k_BT$, respectively.

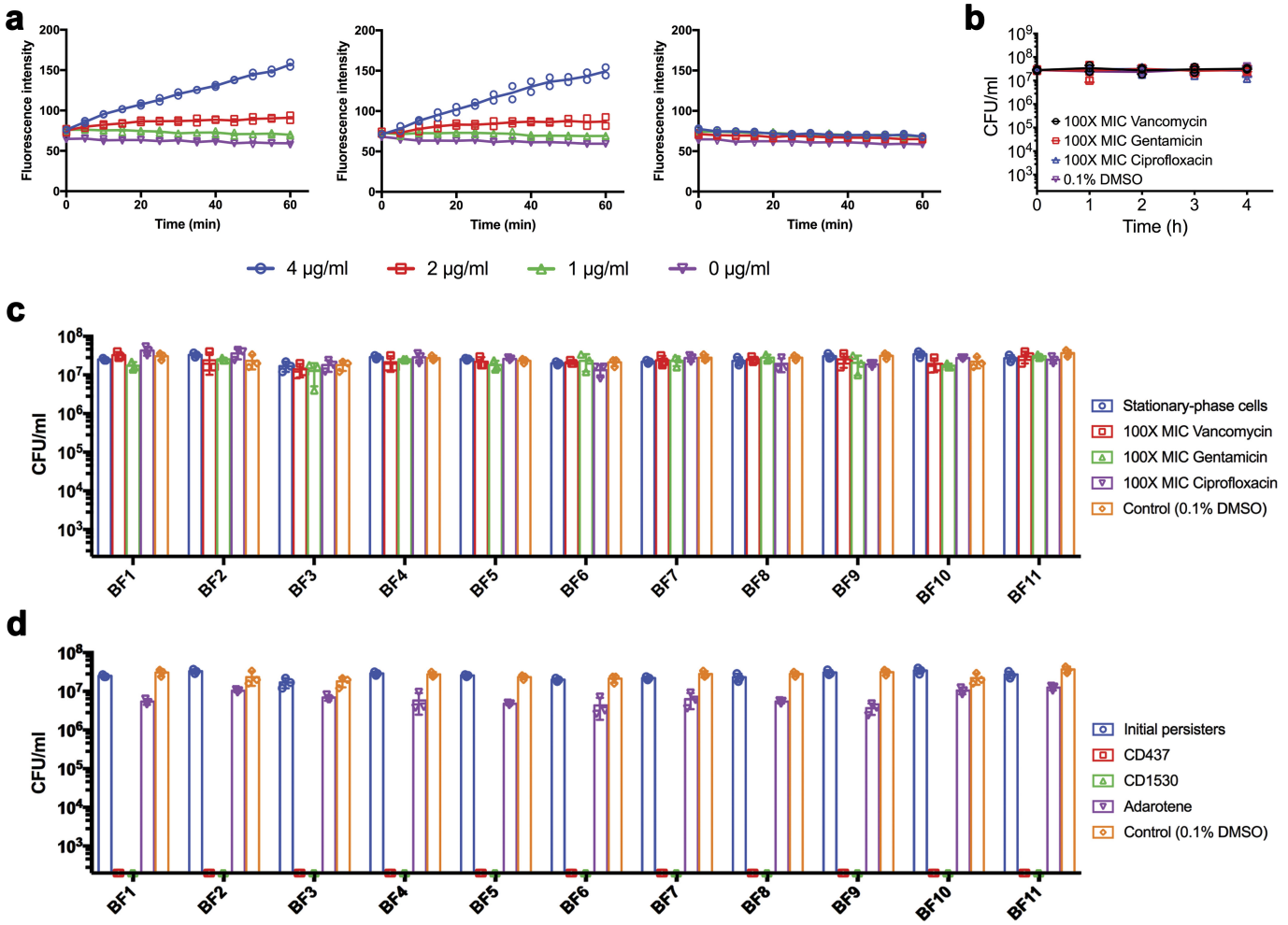

Extended Data Figure 3 | CD437 and CD1530 kill MRSA persisters by inducing membrane permeabilization. a, *S. aureus* MW2 persisters were treated with the indicated concentrations of the retinoids. Membrane permeability was measured spectrophotometrically by monitoring the uptake of SYTOX Green ($\lambda_{ex} = 485$ nm, $\lambda_{em} = 525$ nm) over time. Individual data points ($n = 2$ biologically independent samples) and means are shown; error bars are not shown for clarity. **b**–**d**, Stationary-phase *S. aureus* MW2 (**b**) or stationary-phase cells of 11 clinical *S. aureus* isolates were treated with 100× MIC conventional antibiotics (**c**) or 10× MIC retinoids (**d**) for 4 h. Viability was measured by serial dilution and plating on agar plates. The data points on the *x* axis are below the level of detection (2×10^2 CFU ml^{-1}). **b**–**d**, Individual data points ($n = 3$ biologically independent samples) and mean ± s.d. are shown.

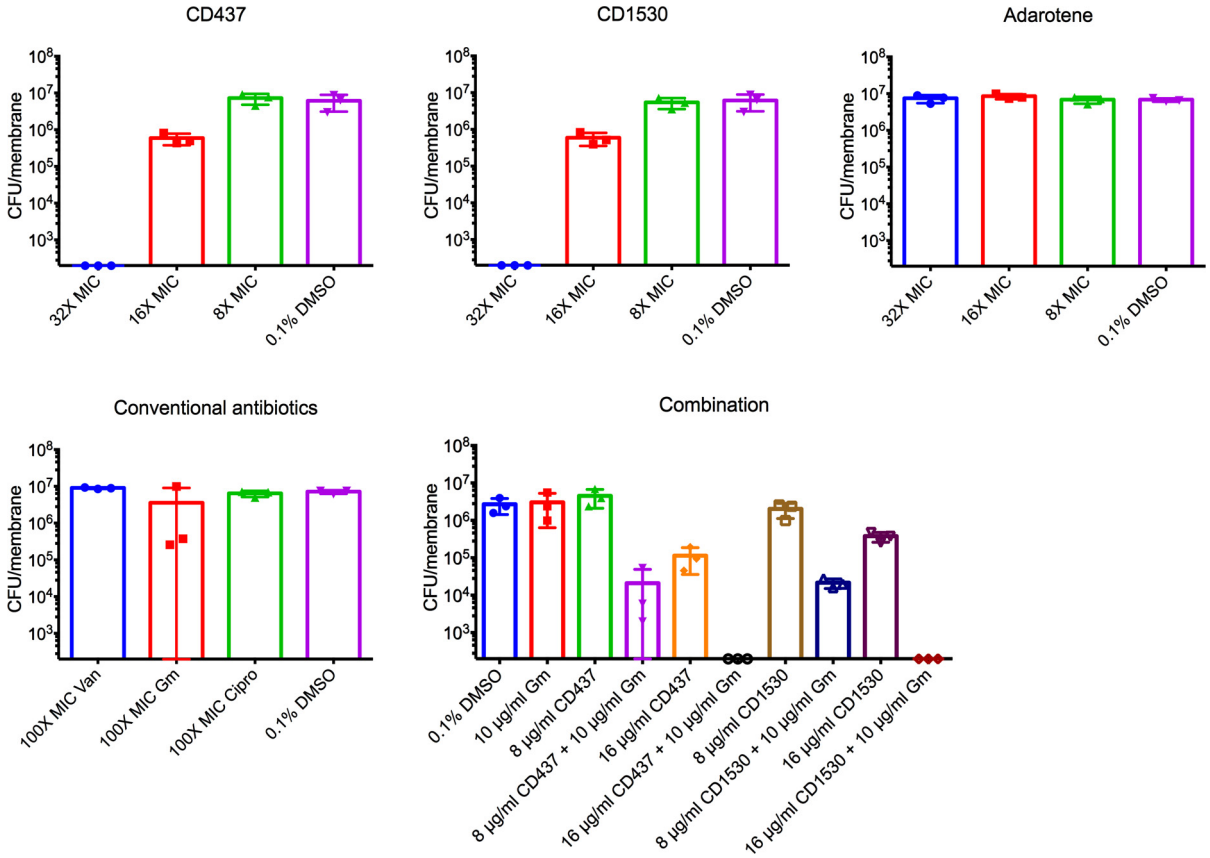

Extended Data Figure 4 | CD437 or CD1530 alone or in combination with gentamicin eliminate persisters formed in MRSA biofilms. MRSA MW2 biofilms formed on 13 mm cellulose ester membranes were treated with the indicated concentrations of retinoids alone or in combination with gentamicin. The number of viable cells in biofilms was measured by CFU counting. The data points on the *x* axis are below the level of detection (2×10^2 CFU ml^{-1}). Individual data points ($n = 3$ biologically independent samples) and mean ± s.d. are shown.

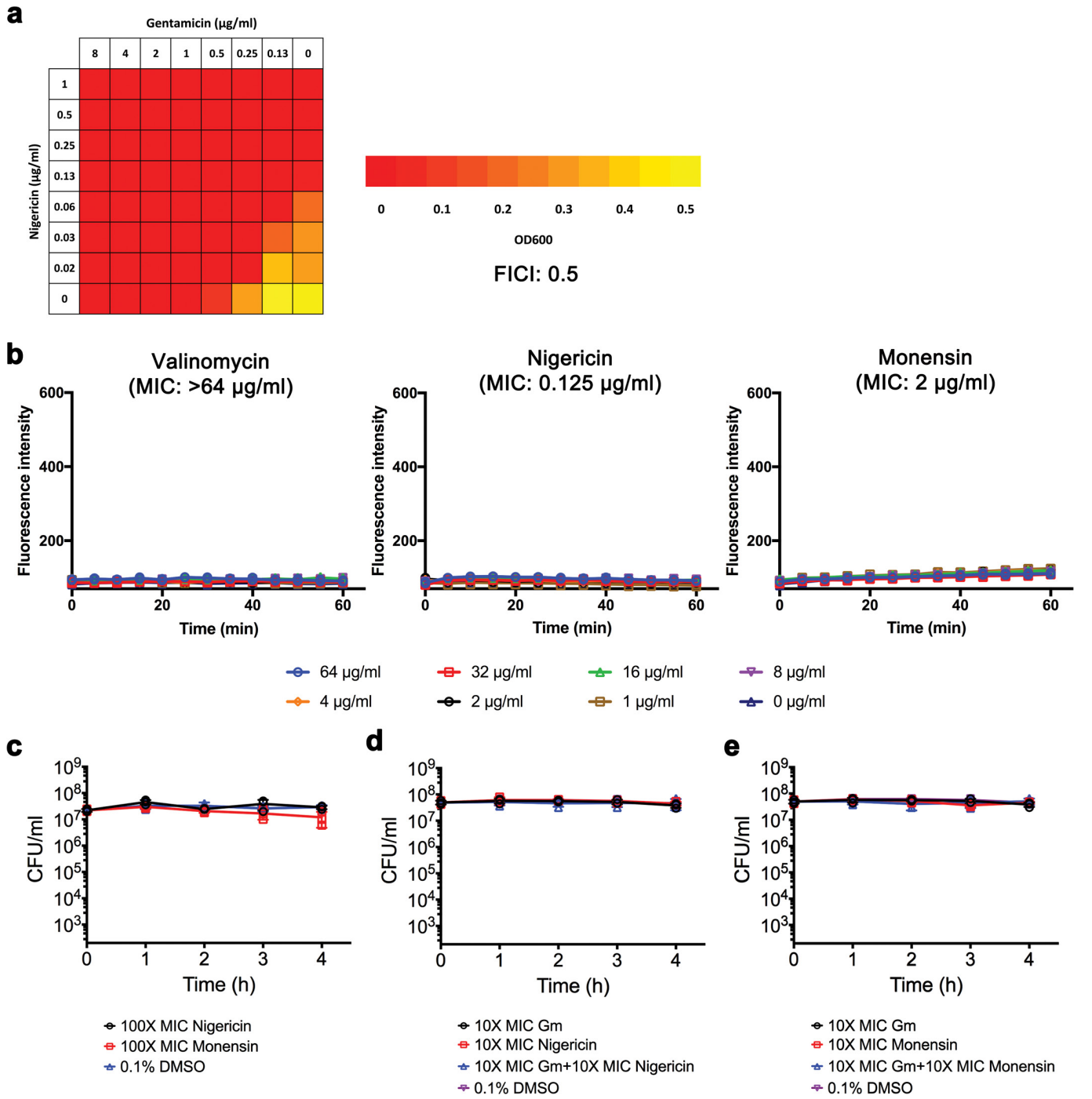

Extended Data Figure 5 | Ionophores do not induce SYTOX Green membrane permeabilization or kill MRSA MW2 persisters. **a**, Synergism between nigericin and gentamicin was evaluated against *S. aureus* MW2 by the fractional inhibitory concentration index (FICI) microdilution checkerboard method. Optical densities at 600 nm were measured after 18 h incubation at 37 °C. Experiments were independently repeated twice with similar results. Synergy, FICI ≤ 0.5; no interaction, $0.5 <$ FICI ≤ 4; antagonism, FICI > 4. **b**, Exponential-phase MW2 cells were treated with the indicated concentrations of valinomycin, nigericin or monensin. Membrane permeability was measured spectrophotometrically by monitoring the uptake of SYTOX Green ($\lambda_{ex} = 485$ nm, $\lambda_{em} = 525$ nm) over time. Individual data points ($n = 2$ biologically independent samples) are shown; error bars are not shown for clarity. **c**–**e**, Stationary-phase *S. aureus* MW2 was treated with the indicated concentrations of ionophores, alone or combined with 10× MIC gentamicin (Gm), or 0.1% DMSO (control) for 4 h. Viability was measured by serial dilution and plating on agar plates. Individual data points ($n = 3$ biologically independent samples) and mean ± s.d. are shown.

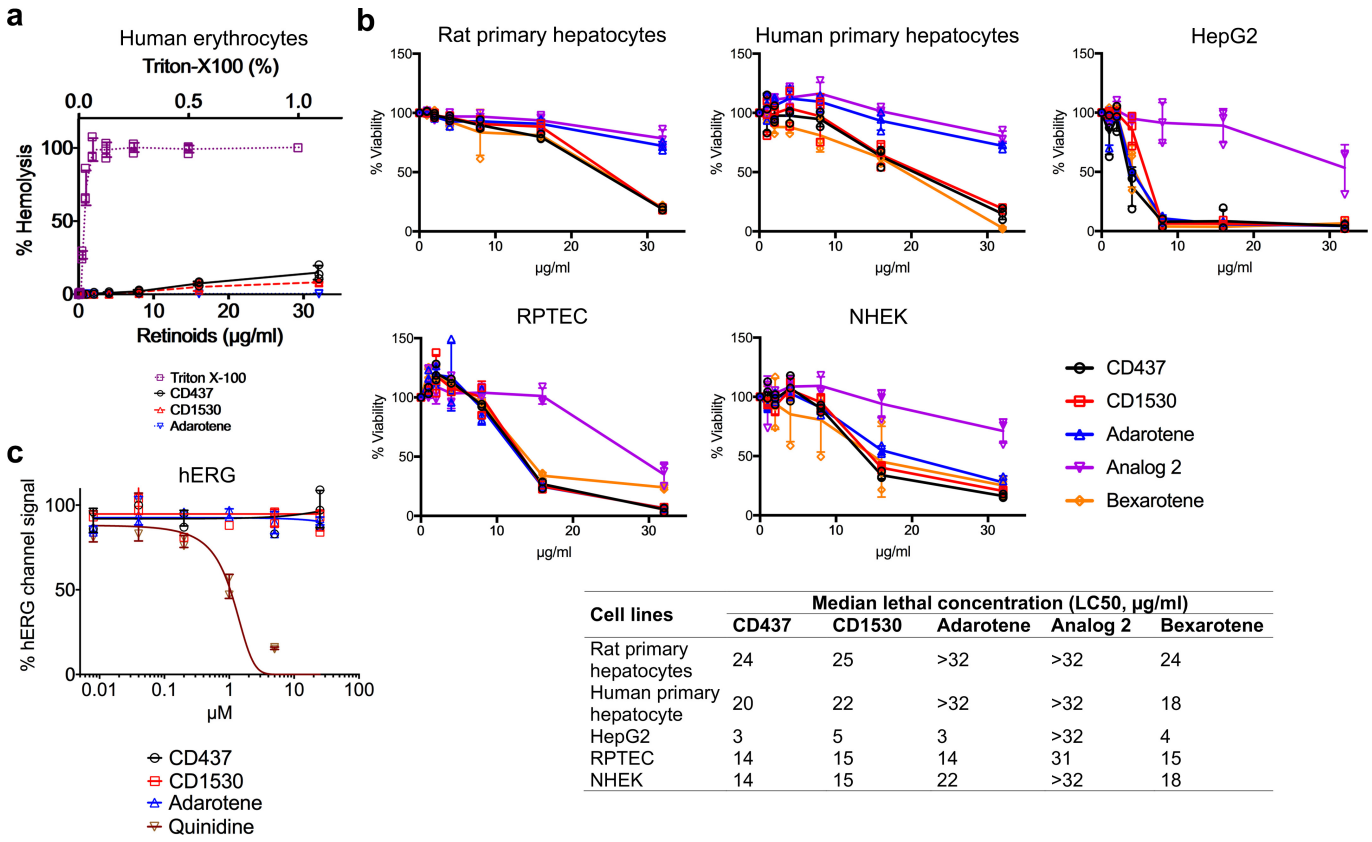

Cell lines	Median lethal concentration (LC50, µg/ml)				
	CD437	CD1530	Adarotene	Analog 2	Bexarotene
Rat primary hepatocytes	24	25	>32	>32	24
Human primary hepatocyte	20	22	>32	>32	18
HepG2	3	5	3	>32	4
RPTEC	14	15	14	31	15
NHEK	14	15	22	>32	18

Extended Data Figure 6 | Evaluation of cytotoxic potentials of retinoids in various cell lines. a, Measurement of haemolytic activity. 2% human erythrocytes were treated with twofold serially diluted concentrations of the retinoids for 1 h at 37 °C. A sample treated with 1% Triton X-100 was used as the control for 100% haemolysis. **b**, Normal rat, human primary hepatocytes, human hepatoma (HepG2) cells, normal human primary renal proximal tubule epithelial cells (RPTEC) or adult normal human epidermal keratinocytes (NHEK) were treated with a range of concentrations of the synthetic retinoids in chemically defined, serum-free medium for 24 h. The FDA-approved antineoplastic retinoid bexarotene was used as a control. Cell viability was calculated on the basis of absorbance readings at 450 nm at 4 h after adding WST-1. **a**, **b**, Individual data points ($n = 3$ biologically independent samples) and mean ± s.d. are shown. **c**, Three synthetic retinoids and the positive control quinidine were tested for inhibition of the hERG potassium channel. Individual data points ($n = 4$ biologically independent samples) and mean ± s.d. are shown. Data are fitted to a standard inhibition curve.

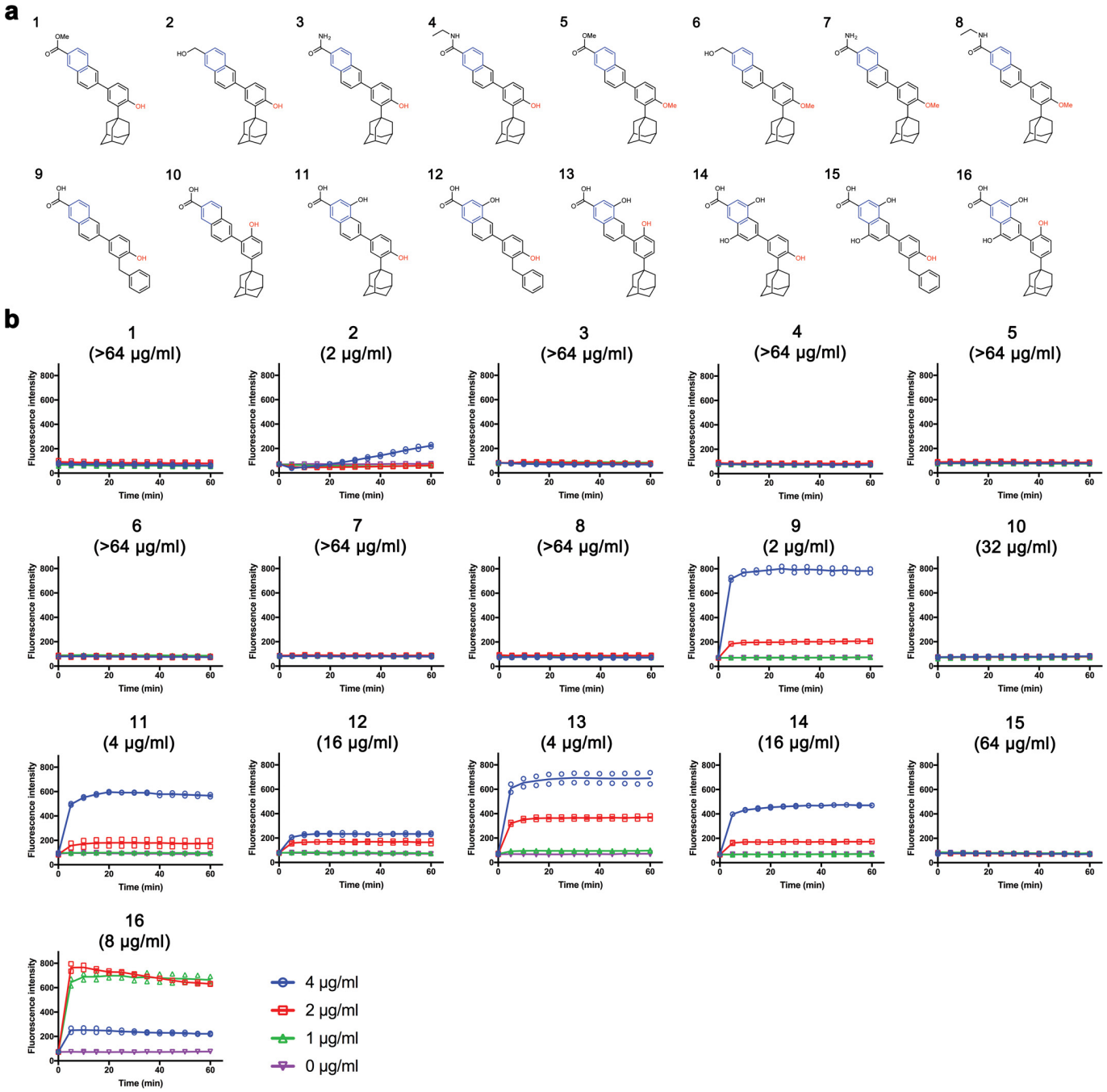

Extended Data Figure 7 | Structure-activity relationships. a, The chemical structures of newly synthesized CD437 analogues. **b**, MICs and membrane permeability were measured for *S. aureus* strain MW2. Membrane permeability was evaluated spectrophotometrically by monitoring the uptake of SYTOX Green ($\lambda_{ex} = 485$ nm, $\lambda_{em} = 525$ nm) over time. Individual data points ($n = 2$ biologically independent samples) and means are shown; error bars are not shown for clarity.

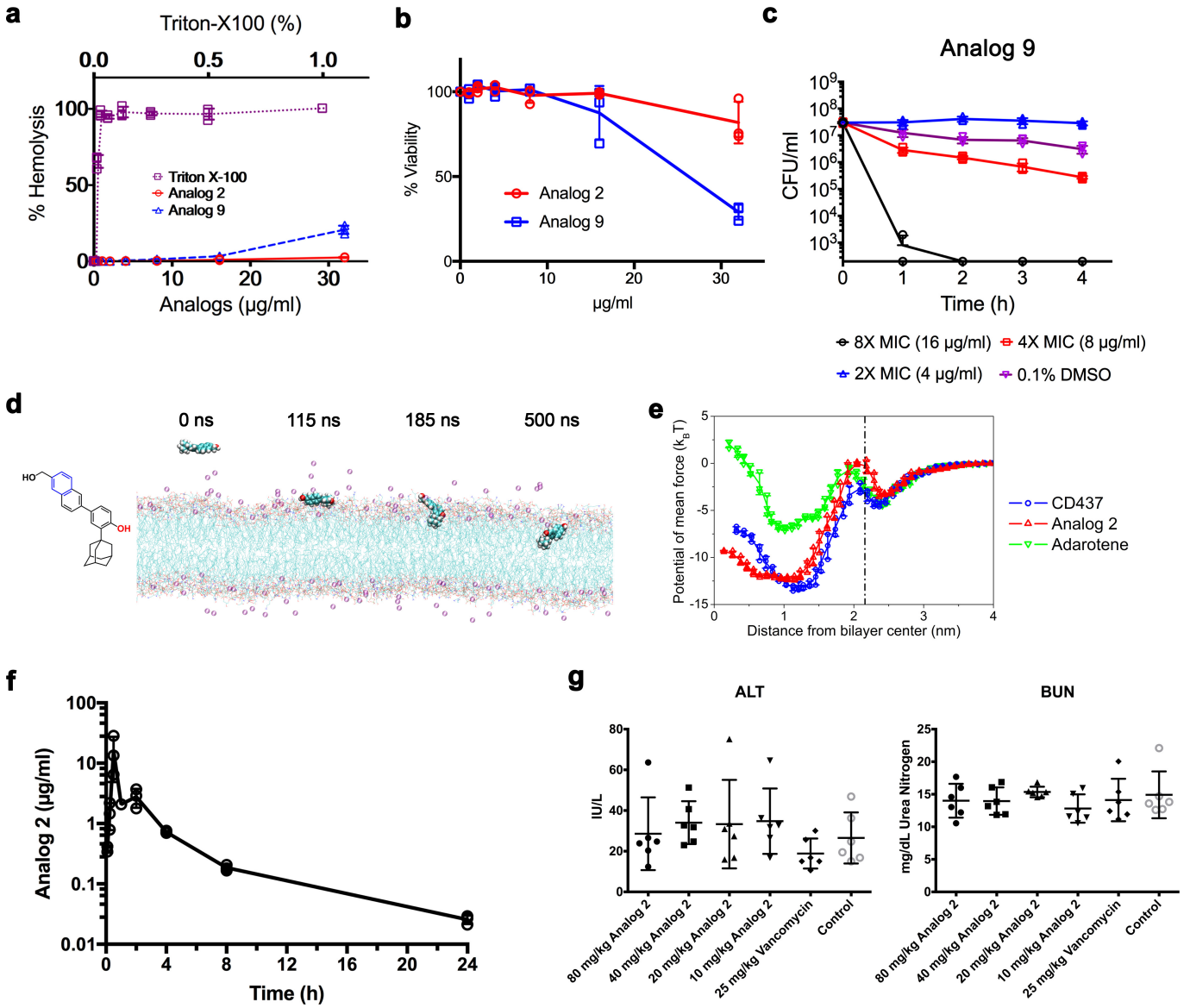

Extended Data Figure 8 | Determination of the biological properties of analogues 2 and 9. a, **b**, Human erythrocytes were treated for 1 h (**a**) and rat primary hepatocytes were treated for 24 h (**b**) with analogues 2 and 9. **c**, MRSA MW2 persisters were treated with analogue 9. The data points on the *x* axis are below the level of detection (2×10^2 CFU ml^{-1}). **a**–**c**, Individual data points ($n = 3$ biologically independent samples) and mean ± s.d. are shown. **d**, Representative configurations of molecular dynamics simulations of analogue 2 interacting with lipid bilayers (108 phosphatidylglycerol lipids, 72 Lys-PG lipids and 10 DPG lipids; see Supplementary Methods for atomic rendering). Simulations were repeated five times with similar results. **e**, Free energy profiles of analogue 2, CD437 and adarotene penetrating the membrane as a function of the distance between the COM of the retinoids and the lipid bilayer. The dot-dashed line marks the membrane surface, averaged from the COM location of phosphate groups in outer leaflet. Individual data points ($n = 3$ independent simulations) and mean ± s.d. are shown. **f**, The plasma concentrations of analogue 2 after a single injection of analogue 2 (20 mg kg^{-1}, i.p., 3 mice per time point) were measured using LC–MS/MS. Pharmacokinetic analysis was conducted using Phoenix WinNonlin software version 6.3. Individual data points ($n = 3$ biologically independent animals) and mean ± s.d. are shown. The determined pharmacokinetic parameters are T_{max} (the time taken to reach the maximum concentration) 0.5 h, C_{max} (maximum concentration observed) 16.14 μg ml^{-1}, AUC_{last} (area under the curve to last time point) 16.38 h·μg ml^{-1}, AUC_{inf} (area under the curve to infinite) 16.54 h·μg ml^{-1}, $t_{1/2}$ (half-life) 4.49 h, clearance 20.16 ml min^{-1} kg^{-1}. **g**, Six mice per group ($n = 6$ biologically independent animals) were treated with control (5% Kolliphor + 5% ethanol, i.p.), vancomycin (25 mg kg^{-1}, i.p.) or analogue 2 (10–80 mg kg^{-1}, i.p.) every 12 h for 3 days. At 12 h after the last treatment, alanine aminotransferase (ALT) and blood urea nitrogen (BUN) were analysed. The concentrations of ALT (in international units per litre, IU l^{-1}) and BUN (mg dl^{-1}) in each mouse serum sample analysed are plotted as individual points and the mean ± s.d. is shown. Control and antibiotic treatments were analysed by one-way ANOVA and post hoc Tukey test, which demonstrated a lack of significant differences ($P > 0.7$ for all ALT and BUN samples).

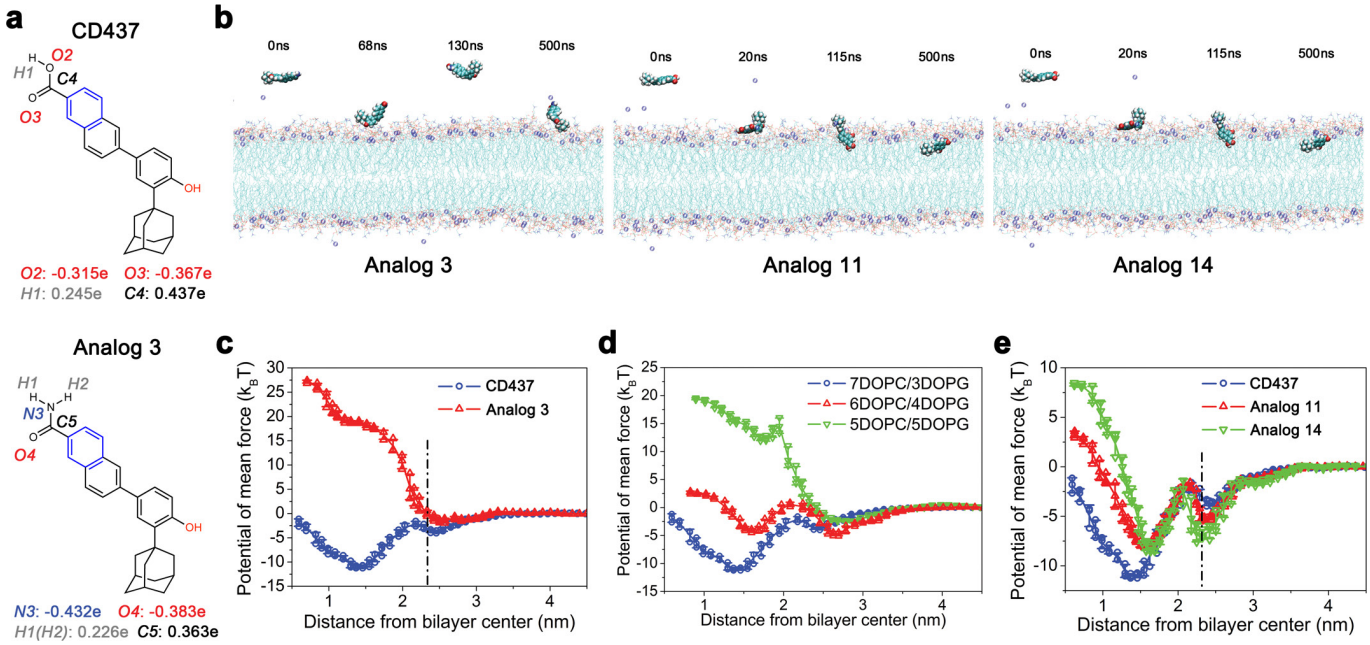

Extended Data Figure 9 | The charges and the number of branch groups affects membrane activity of CD437-like retinoids. a, Comparison of partial atomic charges between CD437 and analogue 3. **b**, Representative configurations of molecular dynamics simulations of analogues 3, 11, and 14 interacting with lipid bilayers (DOPC:DOPG, 7:3). The amide group in analogue 3 is repelled away from the membrane despite the attachment of the hydroxyl group. Atomic rendering is described in Supplementary Methods. Simulations were repeated five times with similar results. **c**, **d**, Free energy profiles of analogue 3 penetrating DOPC:DOPG (7:3) lipid bilayers (**c**) and CD437 penetrating differently charged lipid bilayers (**d**). **e**, Analogues 11 and 14 penetrating DOPC:DOPG (7:3) lipid bilayers as a function of the distance between the COM of the retinoids and the lipid bilayer. The dot-dashed line marks the membrane surface, averaged from the COM location of phosphate groups in the outer leaflet. **c**–**e**, Individual data points ($n = 3$ independent simulations) and mean ± s.d. are shown.

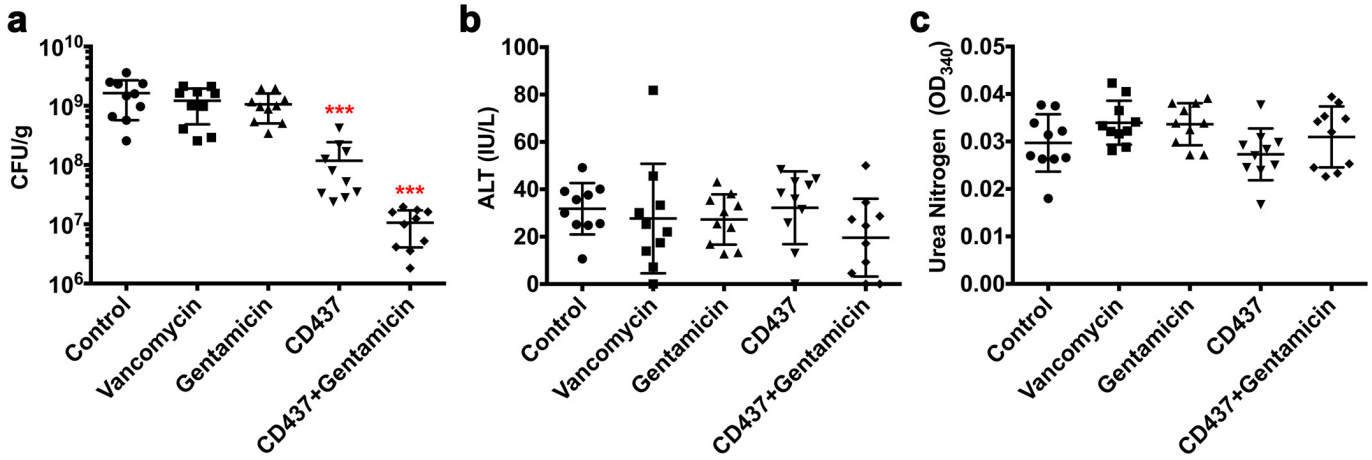

Extended Data Figure 10 | *In vivo* efficacy of CD437 alone or in combination with gentamicin in a deep-seated mouse thigh infection model. We chose a dose of 20 mg kg^{-1} CD437 to test its *in vivo* efficacy in the MRSA mouse deep-seated thigh infection model, because a dose of 20 mg kg^{-1} has shown *in vivo* efficacy in mouse xenograft cancer models[27–29]. Ten MRSA MW2-infected mice per group ($n = 10$ biologically independent animals, see Supplementary Methods) were treated with control (5% Kolliphor + 5% ethanol, i.p.), vancomycin (25 mg kg^{-1}, i.p.), gentamicin (30 mg kg^{-1}, s.c.), CD437 (20 mg kg^{-1}, i.p.), or a combination of CD437 (20 mg kg^{-1}, i.p.) and gentamicin (30 mg kg^{-1}, s.c.) every 12 h for 3 days beginning 24 h after infection. At 12 h after the last treatment, mice were euthanized and their thighs were excised and homogenized, and blood was collected and analysed for ALT and BUN. **a**, CFUs from each mouse thigh are plotted as individual points and the mean ± s.d. for each experimental group is shown. **b**, **c**, Concentration of ALT for each mouse serum sample (**b**) and absorbance of BUN at 340 nm (**c**) are plotted as individual points. The mean ± s.d. for each experimental group is shown. Statistical differences between control and antibiotic treatment groups were analysed by one-way ANOVA and post hoc Tukey test (***$P < 0.0001$).

27. Schadendorf, D. *et al.* Treatment of melanoma cells with the synthetic retinoid CD437 induces apoptosis via activation of AP-1 *in vitro*, and causes growth inhibition in xenografts *in vivo*. *J. Cell Biol.* **135,** 1889–1898 (1996).
28. Langdon, S. P. *et al.* Growth-inhibitory effects of the synthetic retinoid CD437 against ovarian carcinoma models *in vitro* and *in vivo*. *Cancer Chemother. Pharmacol.* **42,** 429–432 (1998).
29. Ponzanelli, I. *et al.* Isolation and characterization of an acute promyelocytic leukemia cell line selectively resistant to the novel antileukemic and apoptogenic retinoid 6-[3-adamantyl-4-hydroxyphenyl]-2-naphthalene carboxylic acid. *Blood* **95,** 2672–2682 (2000).

nature research

Corresponding author(s): Eleftherios Mylonakis

Life Sciences Reporting Summary

Nature Research wishes to improve the reproducibility of the work that we publish. This form is intended for publication with all accepted life science papers and provides structure for consistency and transparency in reporting. Every life science submission will use this form; some list items might not apply to an individual manuscript, but all fields must be completed for clarity.

For further information on the points included in this form, see Reporting Life Sciences Research. For further information on Nature Research policies, including our data availability policy, see Authors & Referees and the Editorial Policy Checklist.

Please do not complete any field with "not applicable" or n/a. Refer to the help text for what text to use if an item is not relevant to your study.
For final submission: please carefully check your responses for accuracy; you will not be able to make changes later.

Experimental design

1. Sample size

Describe how sample size was determined.

For deep-seated mouse thigh infection studies, we performed a single-tailed power analysis using an estimated STD from other mouse MRSA infection studies from our lab and from the literature (Conlon et al., 2013, Nature, 503, 365–70). For MTD and PK studies, No statistical methods were used to predetermine samples size.

2. Data exclusions

Describe any data exclusions.

Two data points in the PK study (ED Fig. 8e) were excluded as outliers based on Grubb's test. (P<0.05). The two outliers were indicated by asterisks in a source data file (ED Fig. 8.xlsx).

3. Replication

Describe the measures taken to verify the reproducibility of the experimental findings.

All attempts were reproducible.

4. Randomization

Describe how samples/organisms/participants were allocated into experimental groups.

No specific randomization method was applied. However, all groups were checked to ensure no significant difference between groups prior to starting experiments. No preference was given to any treatment group in the order of treatment administration.

5. Blinding

Describe whether the investigators were blinded to group allocation during data collection and/or analysis.

During colony counting for in vivo experiments, all samples were numbered and the counting investigator was blinded to the treatment group numbering system.

Note: all in vivo studies must report how sample size was determined and whether blinding and randomization were used.

6. Statistical parameters

For all figures and tables that use statistical methods, confirm that the following items are present in relevant figure legends (or in the Methods section if additional space is needed).

n/a	Confirmed
☐	☒ The exact sample size (*n*) for each experimental group/condition, given as a discrete number and unit of measurement (animals, litters, cultures, etc.)
☐	☒ A description of how samples were collected, noting whether measurements were taken from distinct samples or whether the same sample was measured repeatedly
☐	☒ A statement indicating how many times each experiment was replicated
☐	☒ The statistical test(s) used and whether they are one- or two-sided *Only common tests should be described solely by name; describe more complex techniques in the Methods section.*
☒	☐ A description of any assumptions or corrections, such as an adjustment for multiple comparisons
☐	☒ Test values indicating whether an effect is present *Provide confidence intervals or give results of significance tests (e.g. P values) as exact values whenever appropriate and with effect sizes noted.*
☐	☒ A clear description of statistics including central tendency (e.g. median, mean) and variation (e.g. standard deviation, interquartile range)
☐	☒ Clearly defined error bars in all relevant figure captions (with explicit mention of central tendency and variation)

See the web collection on statistics for biologists for further resources and guidance.

Software

Policy information about availability of computer code

7. Software

Describe the software used to analyze the data in this study.	CellProfiler was used for worm image analysis. CLC Genomics Workbench version 7.0 and the online platform RAST (http://rast.nmpdr.org) were used for analyzing genome sequence. Phoenix WinNonlin (Version 6.3) was used for calculating pharmacokinetic parameters. PASW Statistics 18 and and GraphPad Prism 7 were used for statistic analysis. The GROMACS package (version 4.6.7) used for MD modeling in this work is a open-source code that can be accessed on the public website (http://www.gromacs.org/Downloads).

For manuscripts utilizing custom algorithms or software that are central to the paper but not yet described in the published literature, software must be made available to editors and reviewers upon request. We strongly encourage code deposition in a community repository (e.g. GitHub). *Nature Methods* guidance for providing algorithms and software for publication provides further information on this topic.

Materials and reagents

Policy information about availability of materials

8. Materials availability

Indicate whether there are restrictions on availability of unique materials or if these materials are only available for distribution by a third party.	No unique materials were used.

9. Antibodies

Describe the antibodies used and how they were validated for use in the system under study (i.e. assay and species).	No antibodies were used.

10. Eukaryotic cell lines

a. State the source of each eukaryotic cell line used.	Rat and human primary hepatocytes: the Cell Resource Core at Massachusetts General Hospital (Boston, MA, USA), Human hepatoma HepG2: ATCC (Manassas, VA, USA), Normal human primary renal proximal tubular epithelial cells RPTEC and adult normal human epidermal keratinocytes NHEK: Lonza (Walkersville, MD, USA)
b. Describe the method of cell line authentication used.	All cell lines were authenticated by the vendor. The cell lines were purchased from commercial vendors listed above.
c. Report whether the cell lines were tested for mycoplasma contamination.	Cell lines were routinely tested and found negative for mycoplasma infection by the venders.
d. If any of the cell lines used are listed in the database of commonly misidentified cell lines maintained by ICLAC, provide a scientific rationale for their use.	No commonly misidentified cell lines were used.

Animals and human research participants

Policy information about studies involving animals; when reporting animal research, follow the ARRIVE guidelines

11. Description of research animals

Provide all relevant details on animals and/or animal-derived materials used in the study.	Six-week-old female CD1 ICR outbred mice (20-25 g)

Policy information about studies involving human research participants

12. Description of human research participants

Describe the covariate-relevant population characteristics of the human research participants.	The study did not involve human research participants